SOILS AND FOUNDATIONS Vol. 48, No. 6, 843–850, Dec. 2008
Japanese Geotechnical Society

FINITE ELEMENT LIMIT ANALYSIS OF PASSIVE EARTH RESISTANCE IN COHESIONLESS SOILS

JIM S. SHIAU[i], CHARLES E. AUGARDE[ii], ANDREI V. LYAMIN[iii] and SCOTT W. SLOAN[iii]

ABSTRACT

This note examines the classic passive earth resistance of cohesionless soil by using two newly developed numerical procedures based on finite element formulations of the bound theorems of limit analysis and non-linear programming techniques. Solutions using upper and lower bounds are presented to complement the previous studies of this problem. The parameters studied are soil-wall interface friction, wall inclination, backfill surface configuration and the wall's weight.

Key words: finite elements, limit analysis, nonlinear programming, passive earth pressure, retaining wall **(IGC:** E5/G13/H2)

INTRODUCTION

Passive resistance calculation is required for the design of many geotechnical structures such as retaining walls, sheet piles, bridge abutments, anchor blocks, and group pile caps. Factors that affect the magnitudes of passive pressures have been reviewed recently in Duncan and Mokwa (2001). The most influential parameters for rigid walls are considered to be wall movement, interface friction and adhesion, and wall shape. Traditional analytical approaches, such as those attributed to Rankine and Coulomb and the Log-Spiral method can cope with some, but not all of these parameters.

The Rankine method assumes a smooth wall and the resultant passive force is inclined at an angle equal to the angle of surface inclination behind the wall. In Coulomb's approach, the soil-wall friction angle is assumed to take a value between zero and the internal friction angle of the backfill material. Simple equilibrium is used to determine the resulting passive force. Both methods are developed for granular material and are based on the assumption of plane failure surfaces. However, it is generally recognised that the assumption of a plane failure surface is not reasonable for rough walls. This is especially so for passive cases in which, Coulomb's method may give increasingly unconservative (i.e., unsafe) predictions as the value of soil-wall friction angle increases. To reduce this shortcoming, the Log-Spiral method was developed (Terzaghi, 1943; Terzaghi et al., 1996). Caquot and Kerisel (1948) produced tables and charts of passive pressure coefficients based on this method for cohesionless soil and simple geometries. Duncan and Mokwa (2001) have also recently developed an Excel spreadsheet computer program based on the Log-Spiral method which can accommodate both cohesive and frictional soils, although it is restricted to level ground, a vertical wall, a uniform surcharge, and homogeneous soil. Although conventional displacement finite element (FE) analysis can be used to predict the passive resistance of soils (e.g., Potts and Fourie, 1986; Day and Potts, 1998) these estimates are not rigorous bounds on the true value.

The upper and lower bound theorems of classical plasticity provide rigorous solutions to many problems in geomechanics. Detailed expositions are contained in many references, e.g., Chen (1975). New solutions using the analytical (i.e., non-numerical) upper bound method for estimating passive earth pressure continue to appear in the literature (Soubra and Macuh, 2002). However, since the solution obtained depends on the failure mechanism chosen for the problem, their utility is limited unless a large number of mechanisms are investigated.

To give confidence in the accuracy of the solutions obtained from upper bound calculations, it is desirable to perform lower bound calculations in parallel so that the true result can be bracketed from above and below. Unfortunately, due to the difficulty in constructing statically admissible stress fields in lower bound analysis, this is rarely done in practice. To overcome the difficulty, Lysmer (1970) formulated the lower bound theorem as a rational method for electronic computation. It was developed as a standard linear programming problem and can

[i] Faculty of Engineering and Surveying, University of Southern Queensland, Australia (jim.shiau@usq.edu.au).
[ii] School of Engineering, University of Durham, Durham, UK.
[iii] School of Engineering, University of Newcastle, NSW Australia.
The manuscript for this paper was received for review on February 4, 2008; approved on October 10, 2008.
Written discussions on this paper should be submitted before July 1, 2009 to the Japanese Geotechnical Society, 4-38-2, Sengoku, Bunkyo-ku, Tokyo 112-0011, Japan. Upon request the closing date may be extended one month.

be solved by the Simplex method, which is described in most linear programming textbooks. The method can be used for problems involving arbitrary geometry and stress boundary conditions, but its application is limited. As stated in Lysmer (1970), the method was not always stable. Anderheggen and Knopfel (1972) also developed a numerical procedure, using triangular finite elements and linear programming, to determine the ultimate load of plate structures using both upper and lower bound approaches. The aim was to minimise and maximise a load factor λ.

Following this early work, Sloan (1988, 1989), Sloan and Kleeman (1995), and Lyamin and Sloan (2002a, 2002b) introduced finite element and mathematical programming formulations that permit large two-dimensional problems to be solved efficiently on a standard personal computer. These techniques have removed the need to search for accurate upper bound mechanisms and statically admissible stress fields analytically. The techniques have been used successfully to predict the bearing capacity of layered soils (Shiau et al., 2003), the load capacity of soil anchors (Merifield et al., 2003; Merifield et al., 2005), the stability of tunnels (Sloan and Assadi, 1991), the behaviour of foundations under combined loading (Ukritchon et al., 1998), the bearing capacity of three-dimensional foundations (Salgado et al., 2004; Lyamin et al., 2007), and the formation of sinkholes (Augarde et al., 2003). In this paper, we apply the finite element bound methods to the classical passive earth pressure problem.

PROBLEM DEFINITION AND SOLUTION TECHNIQUES

The passive earth pressure problem considered in this paper is illustrated in Fig. 1. A rigid retaining wall of height H is subjected to a horizontal force that pushes it into the soil. The back of the wall has an angle α to the horizontal and the surface of the backfill slopes at β to the horizontal. The soil is taken to be a cohesionless ($c' = 0$) material with unit weight γ. A fully drained condition is adopted throughout.

It is convenient to use a value of soil-wall friction angle δ to represent wall roughness. For cohesionless soil, $\delta = 0$ models a perfectly smooth wall while $\delta = \phi'$ indicates a perfectly rough wall. The total passive thrust acting on the wall, P_p, is defined in terms of a passive earth pressure coefficient K_p according to

$$P_p = \frac{1}{2} K_p \gamma H^2 \tag{1}$$

The line of action of P_p is inclined at δ to the normal on the back of the wall. Equation (1) is governed by the geometric parameters α and β, the soil-wall friction angle δ, and the backfill frictional angle ϕ'.

Classical limit analysis theory assumes an associated flow rule, which restricts the direction of plastic flow such that $\psi' = \phi'$. The implicit assumption of an associated flow rule in the bound theorems has resulted in some debate on their suitability for frictional soils. Although it is well known that the use of an associated flow rule predicts excessive dilation during shear failure of such a soil, it is less clear whether this feature will have a major impact on the resulting limit load. Indeed, it can be argued that the flow rule will have a major influence on this quantity only if the problem is strongly constrained in a kinematic sense (Davis, 1968). For geomechanics problems which involve a freely deforming ground surface and a semi-infinite domain, the degree of kinematic constraint if often low and it is reasonable to conjecture that the bound theorems will give good estimates of the true limit load. It is also possible to carry out an analysis using a ''residual'' friction angle to model non-associated behaviour, e.g., Shiau et al. (2003) and Michalowski and Shi (1995), however in this paper all analyses assume associated flow.

The upper bound theorem states that the power dissipated by any kinematically admissible velocity field can be equated to the power dissipated by the external loads to give a rigorous upper bound on the true limit load. A kinematically admissible velocity field is one which satisfies compatibility, the flow rule and the velocity boundary

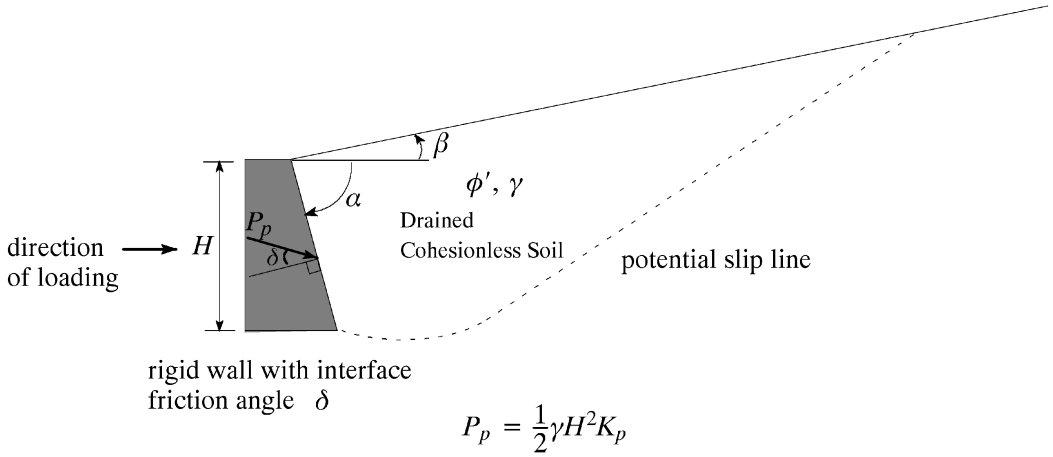

Fig. 1. Problem notation and potential failure mechanism

conditions. In a finite element formulation of the upper bound theorem, the velocity field is modelled using appropriate variables and the optimum (minimum) internal power dissipation is obtained as the solution to a mathematical programming problem.

In the formulation of Lyamin and Sloan (2002b), the upper bound is found by the solution of a nonlinear programming problem. Their procedure uses linear triangles to model the velocity field, and each element is also associated with a constant stress field and a single plastic multiplier rate. The element plastic multipliers do not need to be included explicitly as variables, however, even though they are used in the derivation of the formulation. This is because the final optimisation problem can be cast in terms of the nodal velocities and element stresses alone. To ensure kinematic admissibility, flow rule constraints are imposed on the nodal velocities, element plastic multipliers, and element stresses. In addition, the velocities are matched to the specified boundary conditions, the plastic multipliers are constrained to be non-negative, and the element stresses are constrained to satisfy the yield criterion.

Figure 2 shows a typical finite element mesh for upper bound limit analysis of the problem considered. This mesh comprises 6765 nodes, 2349 triangular elements, and 3325 velocity discontinuities. The bottom and right hand edges of the upper bound meshes used in this study are fixed since it is assumed that the failure mechanism is contained within. This condition is checked for each case and in some instances larger meshes are necessary to ensure that the optimal failure mechanism is captured correctly.

An upper bound solution is obtained by prescribing a unit horizontal translation ($u = +1$) into the soil adjacent to the wall to induce passive failure. To consider the effect of the soil-wall interface, those nodes on the interface boundary are given a different material property from the one adopted for the backfill sand. The upper bound on the passive forces P_p is obtained by equating the power expended by the external loads to the power dissipated internally by plastic deformation. The passive earth pressure coefficients K_p are then found by direct substitution in Eq. (1).

The lower bound limit theorem states that if any equilibrium state of stress can be found which balances the applied loads and satisfies the yield criterion as well as the stress boundary conditions, then the body will not collapse. Stress fields that satisfy these requirements, and thus give lower bounds, are said to be statically admissible. The key idea behind the lower bound analysis applied here is to model the stress field using finite elements and use the static admissibility constraints to express the unknown collapse load as a solution to a mathematical programming problem. For linear elements, the equilibrium and stress boundary conditions give rise to linear equality constraints on the nodal stresses, while the yield condition, which requires all stress points to lie inside or on the yield surface, gives rise to a nonlinear inequality constraint on each set of nodal stresses. The objective function, which is to be maximised, corresponds to the collapse load and is a function of the unknown stresses.

The lower bound formulation in Lyamin and Sloan (2002a) incorporates statically admissible stress discontinuities at all interelement boundaries as well as special extension elements for completing the stress field in an unbounded domain. Although the stress discontinuities increase the total number of variables for a fixed mesh, they also introduce extra ''degrees of freedom'' in the stress field, thus improving the accuracy of the solution. Meshes for the lower bound approach are visually similar to those for the upper bound approach, though they are not shown here. There are two material properties adopted in the analyses; one for the backfill and the other for

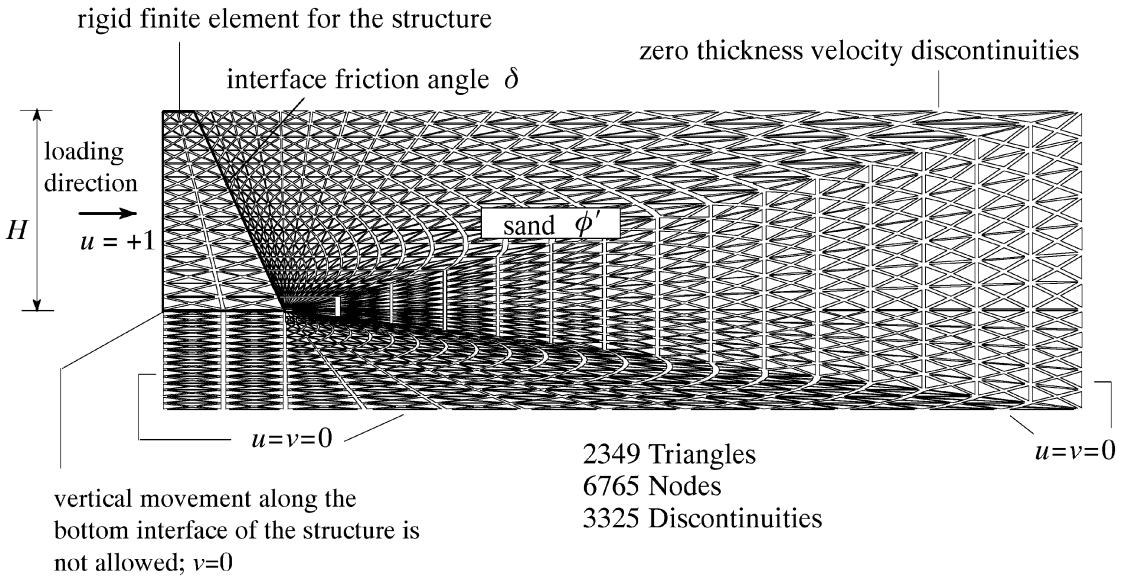

Fig. 2. Typical finite element mesh for upper bound analysis ($\alpha = 60°$, $\beta = 0°$)

the soil-wall interface boundary. To compute the lower bound, the stress field is optimised in a manner that yields the largest passive force on the back of the wall. Once the passive forces are known, the passive earth pressure coefficients K_p are again found by direct substitution in Eq. (1).

Derivation of the finite element formulations of the upper and lower bound theorems are described in detail elsewhere (Lyamin and Sloan, 2002a, 2002b) and will not be repeated here.

RESULTS AND DISCUSSION

Upper bound (UB) and lower bound (LB) estimates of K_p for a rigid retaining wall in a cohesionless soil, under a wide variety of different conditions, are now described. The study covers variations in geometry and soil-wall interface properties. Using traditional approaches, such a wide ranging study would be extremely time-consuming (and probably impossible for the lower bound case). Where possible, these numerical results are compared to solutions obtained by others.

Typical Results

Bounds on K_p for the case of $\phi' = 40°$ are presented in Table 1 where they are compared with other available methods. For a smooth wall ($\delta/\phi' = 0$), a value for K_p of 4.6 is obtained in all methods. As the wall friction is increased, the passive earth pressure coefficients for the numerical upper and lower bounds increase and the bounds typically bracket the true estimates within $\pm 7\%$ (UB-LB/2LB). Note that both the Log-Spiral limit equilibrium methods by Caquot and Kerisel (1948) and Duncan et al. (2001) predict higher values of K_p than our numerical UBs except for the fully rough case ($\delta/\phi' = 1$). The reason for this discrepancy is not clear, however, the bounding results give a very clear indication of the true K_p values. In design practice, the interface friction angle (wall roughness) is typically one half to two thirds of the sand friction angle.

Using the same finite element meshes, a wide range of analyses have been performed for various values of friction angle ϕ'. Numerical results from these analyses are presented in Table 2 and Fig. 3. In general, the numerical limit analyses provide excellent estimates of the passive earth pressure at failure for low soil friction angles, but the bounding accuracy decreases for cases with $\phi' > 40°$ and larger values of soil-wall friction angles. Overall, the numerical results presented in Fig. 3 bracket the true estimates within $\pm 10\%$.

Figure 4 shows the velocity diagrams from UB calculations for various values of δ/ϕ' with $\phi' = 35°$. The plots clearly demonstrate the improved passive resistance that results from increasing the soil-wall friction. They also show the potential errors inherent in the assumption of a plane failure surface. Interestingly, a typical Rankine solution ($\delta/\phi' = 0$) is also obtained in this figure with a plane failure surface intersecting at an angle of approxi-

Table 1. Results comparison ($\alpha = 90°$, $\beta = 0°$, $\phi' = 40°$)

δ/ϕ'	$K_p = 2P_p/\gamma H^2 = 2P_{p,h}/\gamma H^2 \cos\delta$						
	Coulomb Theory	Caquot and Kerisel (1948)	Log Spiral Method (Duncan et al., 2001)	Sokolovski (1960)	Upper Bound (Chen, 1975)	Upper Bound This paper	Lower Bound This paper
0	4.60	4.59	4.60	4.60	4.60	4.61 (16)	4.60 (16)
1/3	8.15	8.13	8.17	—	7.73	7.79 (20)	6.87 (15)
1/2	11.77	10.36	10.50	9.69	10.08	10.03 (35)	8.79 (17)
2/3	18.72	13.10	13.08	—	13.09	12.87 (60)	11.30 (15)
1	92.72	17.50	17.50	18.20	20.91	20.10 (64)	18.64 (24)

Note: The values in parentheses are CPU time in seconds for a Pentimum IV 2.6 GHz desktop personal computer

Table 2. Passive pressure coefficients ($\alpha = 90°$, $\beta = 0°$)

δ/ϕ'	$K_p = 2P_p/\gamma H^2 = 2P_{p,h}/\gamma H^2 \cos\delta$											
	$\phi' = 20°$		$\phi' = 25°$		$\phi' = 30°$		$\phi' = 35°$		$\phi' = 40°$		$\phi' = 45°$	
	LB	UB	LB	UB	LB	UB	LB	UB	LB	UB	LB	UB
0	2.04	2.05	2.46	2.48	3.00	3.01	3.70	3.72	4.60	4.62	5.82	5.86
1/3	2.32	2.42	2.93	3.11	3.78	4.10	5.00	5.58	6.87	7.79	9.69	11.41
1/2	2.50	2.62	3.26	3.48	4.37	4.76	6.08	6.77	8.79	10.03	13.42	15.85
2/3	2.67	2.82	3.59	3.86	5.02	5.49	7.32	8.17	11.30	12.87	19.08	22.03
1	3.02	3.21	4.33	4.70	6.58	7.14	10.99	11.50	18.64	20.10	38.52	45.14

Note: LB andUB are lower and upper bound results

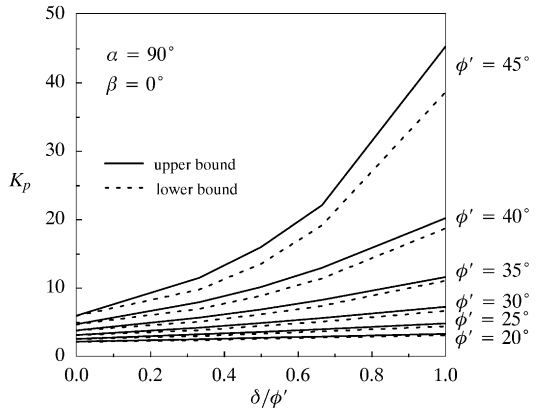

Fig. 3. Typical upper and lower bound results ($\alpha = 90°$, $\beta = 0°$)

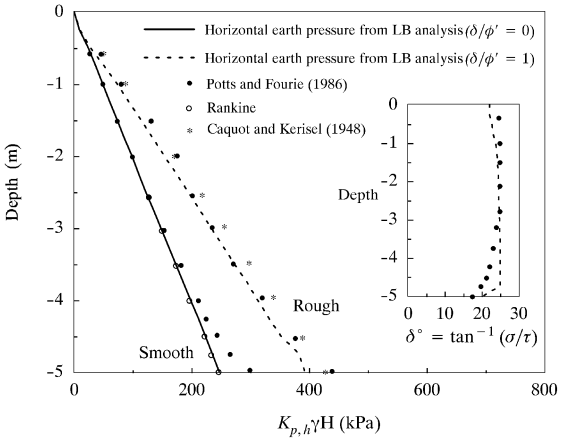

Fig. 5. Comparison of horizontal earth pressure distributions on smooth and rough walls ($\alpha = 90°$, $\beta = 0°$, $\phi' = 25°$)

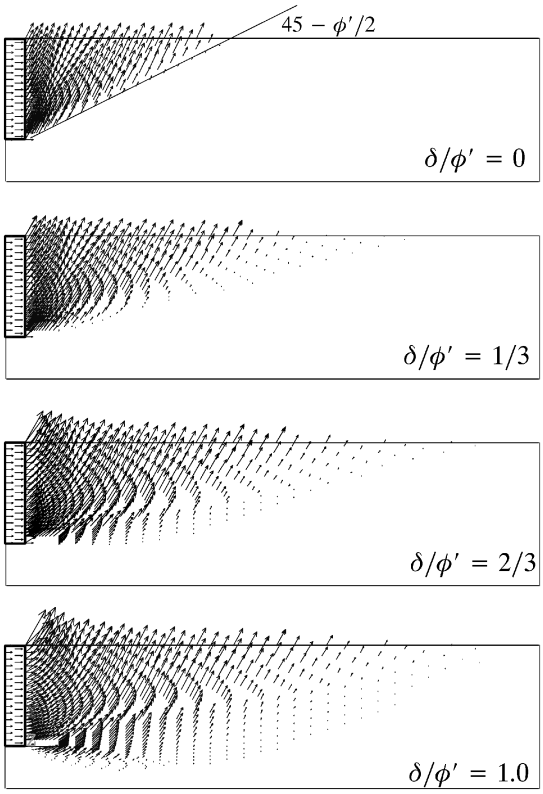

Fig. 4. Velocity diagrams for various values of δ/ϕ' ($\alpha = 90°$, $\beta = 0°$, $\phi' = 35°$)

mately $45° - \phi'/2$ to the horizontal backfill. Note that the results presented here are for heavy walls as vertical movement is prevented.

A comparison of the distribution of passive earth pressure is shown in Fig. 5. The LB passive pressures are plotted for a backfill friction angle $\phi' = 25°$ with both smooth walls (solid line) and rough walls (dotted line). Those obtained by the displacement finite element method (Potts and Fourie, 1986) and the Log-spiral limit equilibrium method (Caquot and Kerisel, 1948) are also plotted. The LBs agree well with these methods. Note that, for the rough wall case, a slightly disparity is observed for the boundary nodes near the bottom of the wall. Further investigation of the developed wall friction (computed as $\delta = \tan^{-1}(\tau/\sigma)$ from the lower bound results) along the interface boundary indicates that the soil-wall friction was not fully developed due to the complex stress condition near this area. A similar observation is made in Potts and Fourie (1986).

Effect of Backfill Slope

Recent experimental data on the passive earth pressure with an inclined surface by Fang et al. (1997) shows that normalized wall movement S/H (where S is the horizontal wall movement and H is the wall height) required to reach a passive state increases with an increasing backfill inclination and that the earth pressure distributions are essentially linear at each stage of wall movement. The relationship between the coefficient of horizontal passive earth pressure $K_{p,h}$ and the backfill slope angles β are shown for each stage of wall movement in Fig. 6. Also plotted in this figure are our numerical bounds. It can be seen that the bounds agree well with the experimental data for $S/H = 0.2$, but not with the failure state reported in their paper. The disparity between the results could be attributed to the assumption of small strain in the limit theorems, compared to the large deformations occurring in the experimental work.

Figure 7 shows the contoured velocity field from the UB calculations for various values of β. Letting (u, v) denote the horizontal and vertical velocity components, the contoured velocity field in Fig. 7 shows the "resultant" velocity; i.e., $\sqrt{u^2 + v^2}$. Note that the precise values of the velocity countours are not important, and are thus not shown in the figure. Notably, the failure surface changes from plane to curved and the proportion of soil at failure reduces when the angle is increased from $-10°$ to $+20°$.

Effect of Wall Inclination

The numerical results above are limited to vertical walls ($\alpha = 90°$). We now move to inclined walls (i.e., inclined rear surfaces such as might be found on a gravity wall).

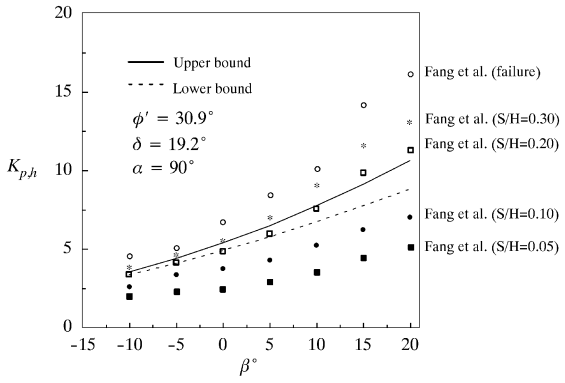

Fig. 6. Comparisons with experimental results (after Fang et al., 1997)

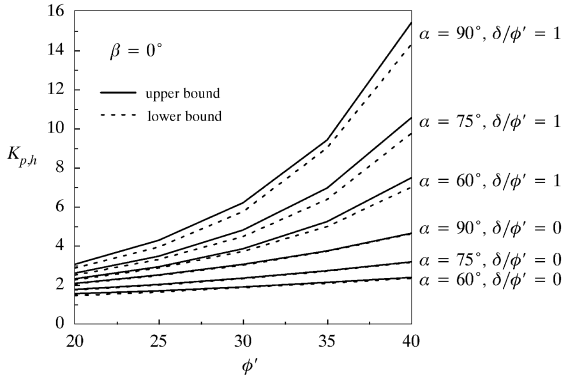

Fig. 8. Upper and lower bound results for studying the effect of wall inclination ($\beta = 0°$)

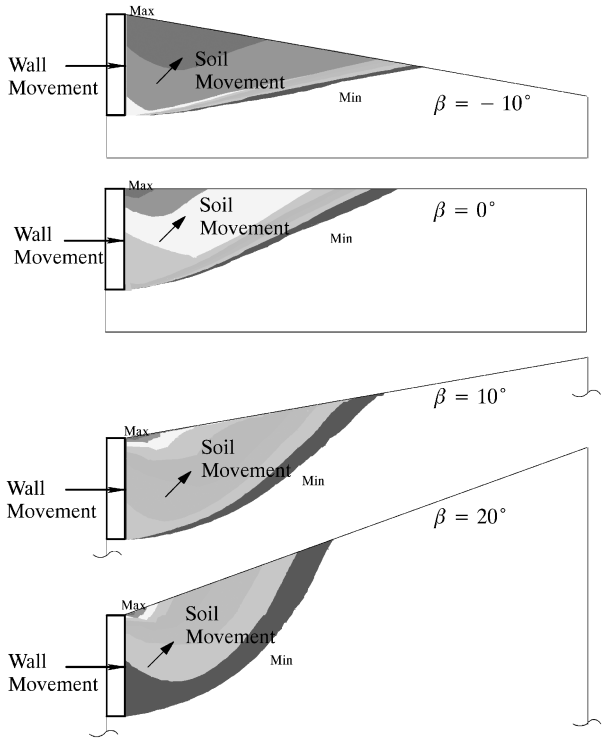

Fig. 7. Contours of velocity fields for various values of β ($\alpha = 90°$, $\phi' = 30.9°$, $\delta = 19.2°$)

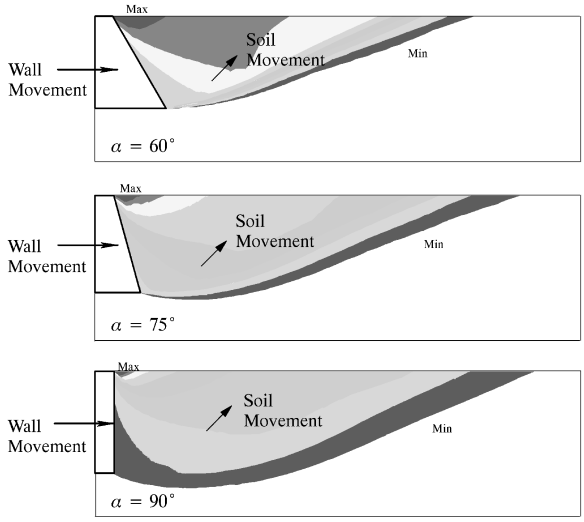

Fig. 9. Contours of velocity fields for various values of α ($\beta = 0°$, $\phi' = 40°$, $\delta/\phi' = 1$)

Figure 8 shows UBs and LBs for perfectly smooth and perfectly rough walls with $\alpha = 60°$, 75°, and 90° and $\phi' = 20°$, 30° and 40°. The horizontal passive earth pressure factor $K_{p,h}$ decreases as the angle α is decreased. Considering the case of a perfectly rough wall with $\phi' = 40°$, for example, $K_{p,h}$ decreases by a factor of approximately 2 as α is decreased from 90° to 60°. Note that the same factor is obtained for the case with a perfectly smooth wall although less passive resistance is expected.

Figure 9 shows the velocity fields for three different wall inclination angles $\alpha = 60°$, 75°, and 90° from our upper bound analyses. A wall with $\alpha = 60°$ leads to the shortest length of slip and low passive resistance. An increase in α is therefore expected to raise passive resistance by enlarging the failure mechanism, thus resulting in a longer slip surface and mobilizing more of the available shear strength.

Effect of Wall Weight

Most current practice in the computation of passive earth pressure asssumes horizontal wall movement only. In practice, soil adjacent to the wall will move both horizontally and vertically, and consequently a net shear force will develop along the soil-wall interface (Duncan and Mokwa, 2001). The passive force will therefore act at an angle to the normal of the soil-wall interface boundary. In reality, it is both the vertical component of the passive force and the body weight of the wall that control the wall movement. In the case of light wall where its weight is much smaller than the potential vertical component of the passive force, the soil-structure interface angle δ may not be fully mobilised, possibly resulting in a situation that both the wall and the soil move together during the process of failure.

An UB mesh similar to Fig. 2 is used to study this effect, however, unlike the mesh for the lower bound analysis, the retaining wall is modelled with rigid elements and the unit weight of the wall is included in the

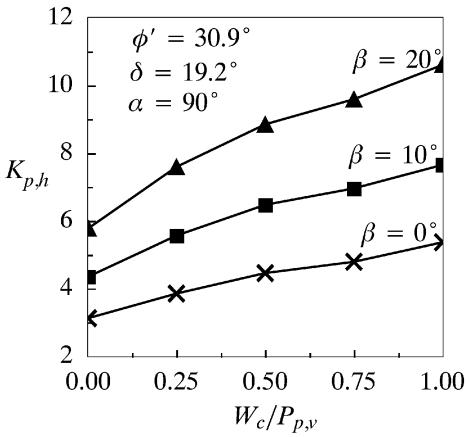

Fig. 10. Effect of wall's weight

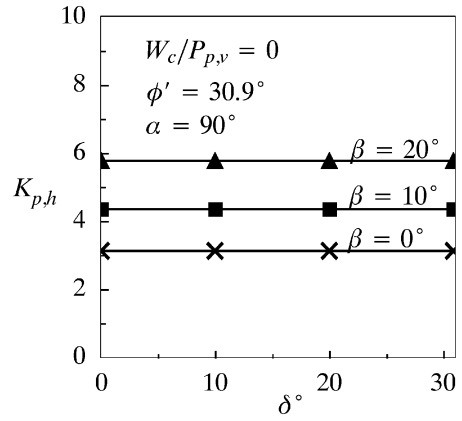

Fig. 11. Effect of soil-wall friction angle on weightless walls

computation. Nodes at the base of the wall are allowed to move freely in both horizontal and vertical directions so that the interaction between the wall and the soil can be modelled.

For the particular case of $\phi' = 30.9°$, $\delta = 19.2°$, and $\alpha = 90°$, Fig. 10 shows that $K_{p,h}$ increases by a factor of roughly 1.7 as the normalized wall weight $W_c/P_{p,v}$ (where $P_{p,v}$ is the pre-estimated passive force in the vertical direction) is increased from 0 to 1.0. It is clear that more interface friction is mobilised as the body weight of the wall is increased, causing an increase in the passive resistance. Therefore, the classical methods that assume a heavy wall may lead to over-estimates of passive pressure. Note that the values of $K_{p,h}$ for the three backfill angles $\beta = 0°$, 10°, and 20° at $W_c/P_{p,v} = 1.0$ are equal to 5.36, 7.64, and 10.60 respectively. These $K_{p,h}$ values are very close to those results previously shown in Fig. 6 where a heavy wall was assumed. Clearly, the wall moves horizontally for $W_c \geq P_{p,v}$ and the computed passive resistance is the same as that in the traditional approach.

Finally keeping all other parameters the same, but modelling a weightless wall ($W_c/P_{p,v} = 0$) and varying soil-wall friction leads to the UBs shown in Fig. 11. These results suggest the wall friction has no effect on the passive resistance when $W_c/P_{p,v} = 0$. The value of $K_{p,h}$ remains constant as δ is increased, indicating that the shear stresses along the soil-wall boundary cannot be developed. This effect is also illustrated in Fig. 12 where the deformed shapes and contours of velocity fields are shown graphically. As expected, the weight of the wall has a greater influence on the soil-structure behaviour of passive walls. The failure mechanism is enlarged as the value of $W_c/P_{p,v}$ increases, thus causing an increase in the passive force. Note also that slippage between the wall and backfill soil increases as $W_c/P_{p,v}$ is increased, thus mobilising more of the interface shear force and causing a curved surface in the failure mechanism.

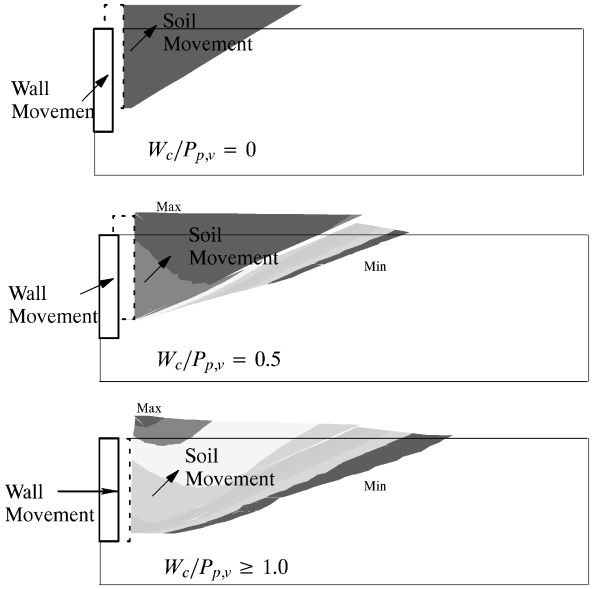

Fig. 12. Deformed shapes and contours of velocity fields for various values of $W_c/P_{p,v}$ ($\alpha = 90°$, $\beta = 0°$, $\phi' = 30.9°$, $\delta = 19.2°$)

CONCLUSIONS

Plasticity solutions using finite element upper and lower bounds are presented in this note to complement the previous studies of this problem. Consideration has been given to the effect of soil-structure interface friction angle, sloping backfill, wall inclination, and the weight of the retaining structure. Results have been presented as passive earth pressure coefficients to facilitate their use in practical designs. Assuming the backfill soil obey an associated flow rule, the solutions presented in this paper bracket the passive earth pressure to within 10% or better and are thus sufficiently accurate for design purposes.

REFERENCES

1) Anderheggen and Knopfel (1972): Finite element limit analysis using linear programming, *International Journal of Solids and Structures*, **8**, 1413–1431.
2) Augarde, C. E., Lyamin, A. V. and Sloan, S. W. (2003): Prediction of undrained sinkhole collapse, *Journal of Geotechnical and Geoenvironmental Engineering*, ASCE, **129**(3), 197–205.
3) Caquot, A. and Kerisel, J. (1948): *Tables for the Calculation of Passive Pressure, Active Pressure and Bearing Capacity of Founda-*

tions, Gauthier-Villars, Paris.
4) Chen, W. F. (1975): *Limit Analysis and Soil Plasticity*, Elsevier, Amsterdam.
5) Davis, E. H. (1968): Theories of plasticity and the failure of soil masses, *Soil Mechanics: Selected Topics* (ed. by I. K. Lee.), Butterworth, London, England, 341–380.
6) Day, R. A. and Potts, D. M. (1998): The effect of interface properties on retaining wall behaviour, *International Journal for Numerical and Analytical Methods in Geomechanics*, **22**, 1021–1033.
7) Duncan, J. M. and Mokwa, R. (2001): Passive earth pressures: theories and tests, *Journal of Geotechnical and Geoenvironmental Engineering*, ASCE, **127**(3), 248–257.
8) Fang, Y. S., Chen, J. M. and Chen, C. Y. (1997): Earth pressures with sloping backfill, *Journal of Geotechnical and Geoenvironmental Eng.*, ASCE, **123**(3), 250–259.
9) Lee, I. K. and Herrington, J. R. (1972): A theoretical study of the pressures acting on a rigid wall by a sloping earth or rock fill, *Géotechnique*, **22**(1), 1–26.
10) Lyamin, A. V., Salgado, R., Sloan, S. W. and Prezzi, M. (2007): Two-and three-dimensional bearing capacity of footings on sand, *Géotechnique*, **57**(8), 647–662.
11) Lyamin, A. V. and Sloan, S. W. (2002a): Lower bound limit analysis using nonlinear programming, *International Journal for Numerical Methods in Engineering*, **55**, 573–611.
12) Lyamin, A. V. and Sloan, S. W. (2002b): Upper bound limit analysis using linear finite elements and nonlinear programming, *International Journal for Numerical and Analytical Methods in Geomechanics*, **26**, 181–216.
13) Lysmer (1970): Limit analysis of plane problems in solid mechanics, *Journal of the Soil Mechanics and Foundations Division, Proc. American Society of Civil Engineers*, **96**, 1311–1334.
14) Merifield, R. S., Lyamin, A. V., Sloan, S. W. and Yu, H. S. (2003): Three-dimensional lower bound solutions for stability analysis of plate anchors in clay, *Journal of Geotechnical and Geoenvironmental Engineering*, ASCE, **129**(3), 243–253.
15) Merifield, R. S., Lyamin, A. V. and Sloan, S. W. (2005): The stability of inclined plate anchors in purely cohesive soil, *Journal of Geotechnical and Geoenvironmental Engineering*, ASCE, **131**(6), 792–799.
16) Michalowski, R. L. and Shi, L. (1995): Bearing capacity of footings over two-layer foundation soils, *Journal of Geotechnical Eng.*, ASCE, **121**(5), 421–428.
17) Potts, D. M. and Fourie, A. B. (1986): A numerical study of the effects of wall deformation on earth pressures, *International Journal for Numerical and Analytical Methods in Geomechanics*, **10**, 383–405.
18) Salgado, R., Lyamin, A. V., Sloan, S. W. and Yu, H. S. (2004): Two-and three-dimensional bearing capacity of foundations in clay, *Géotechnique*, **54**(5), 297–306.
19) Shiau, J. S., Lyamin, A. V. and Sloan, S. W. (2003): Bearing capacity of a sand layer on clay by finite element limit analysis, *Canadian Geotechnical Journal*, **40**, 900–915.
20) Sloan, S. W. (1988): Lower bound limit analysis using finite elements and linear programming, *International Journal for Numerical and Analytical Methods in Geomechanics*, **12**, 61–67.
21) Sloan, S. W. (1989): Upper bound limit analysis using finite elements and linear programming, *International Journal for Numerical and Analytical Methods in Geomechanics*, **13**, 263–282.
22) Sloan, S. W. and Assadi, A. (1991): Undrained stability of a square tunnel in a soil whose strength increases linearly with depth, *Computers and Geotechnics*, **12**(4), 321–346.
23) Sloan, S. W. and Kleeman, P. W. (1995): Upper bound limit analysis using discontinuous velocity fields, *Computer Methods in Applied Mechanics and Engineering*, **127**, 293–314.
24) Sokolovski, V. (1960): *Statics of Soil Media*, Butterworths Publications, London.
25) Soubra, A. H. and Macuh, B (2002): Active and passive earth pressure coefficients by a kinematical approach, *Geotechnical Enginnering, Proc. Institution of Civil Engineers*, **155**(2), 119–131.
26) Terzaghi, K. (1943): *Theoretical Soil Mechanics*, John Wiley and Sons, Inc., New York.
27) Terzaghi, K., Peck, R. B. and Mezri, G. (1996): *Soil Mechanics in Engineering Practice*, 3rd Ed., John Wiley and Sons, Inc., New York.
28) Ukritchon, B., Whittle, A. J. and Sloan, S. W. (1998): Undrained limit analyses for combined loading of strip footings on clay, *Journal of Geotechnical and Geoenvironmental Engineering*, ASCE, **124**(3), 265–276.